2.10 Beam Diagnostics and Control

2.10.1 Introduction

The end product of the ERL is the x-ray beam produced in the undulators, and the task of the beam diagnostics and control system is to stabilize the ERL beam to the needed accuracy. The most stringent beam requirements are for the beam in the 25 m long undulator with:

- $\sigma_x = 0.3\,\mu$m (horizontal beam position jitter)
- $\sigma_y = 0.3\,\mu$m (vertical beam position jitter)
- $\delta E/E = 2 \times 10^{-4}$ (beam energy spread)
- $\sigma_{x,y,\mathrm{rms}} = 0.3\,\mu$m (beam size variation)
- $\sigma_z = c \times 20\,$fs (bunch length variation)
- $\sigma_t = 20\,$fs (arrival-time variation)

While these tolerances are tight, they are not beyond the state of the art in presently operating storage rings and FELs. As much as possible, existing designs for the various beam diagnostics and control systems will be used in the ERL. Therefore none of the proposed systems should need an extensive research and development program to achieve their parameters.

The ERL's main distinction is the presence of two beams in the Linac structures that need to be individually diagnosed and controlled. The fact that the two beams generate a 2.6 GHz signal in the beam position monitors, in addition to the 1.3 GHz signal can be used to determine the positions of the two beams separately.

The following sections describe the components of the beam diagnostics and control system. The ERL has five different operating modes and the system must accommodate each of these modes. The first section describes the start-up procedure, and is followed by the beam position monitoring system. The various feedback systems are then described, and the likely seismic environment at the ERL completes this chapter.

2.10.2 Beam position measurement system

The conceptual design for the beam position monitor (BPM) system is based on experience from the use of three generations of BPM processors, capable of bunch-by-bunch and turn-by-turn position measurements in CESR and a simple adaptation of these processors for CW use with the ERL prototype injector. The basic block diagram for the beam position monitor system is shown in Fig. 2.10.1. A vacuum chamber with either four striplines or four button pickups is the element employed as the beam position detector where approximately 90 % of the BPMs will be button detectors and the remainder will be more sensitive stripline detectors. Since the beam has a 1.3 GHz CW repetition frequency f_0, there will be a 1.3 GHz band pass filter with 50 MHz bandwidth for each of the signals. This will produce a 1.3 GHz signal averaged over about 26 bunches. Each filtered signal will then be down converted to 12.5 MHz and fed into one of the four input ports of the BPM electronics. The input analog board will have the ability to change its gain over a range of nearly 200. The signal will be sampled

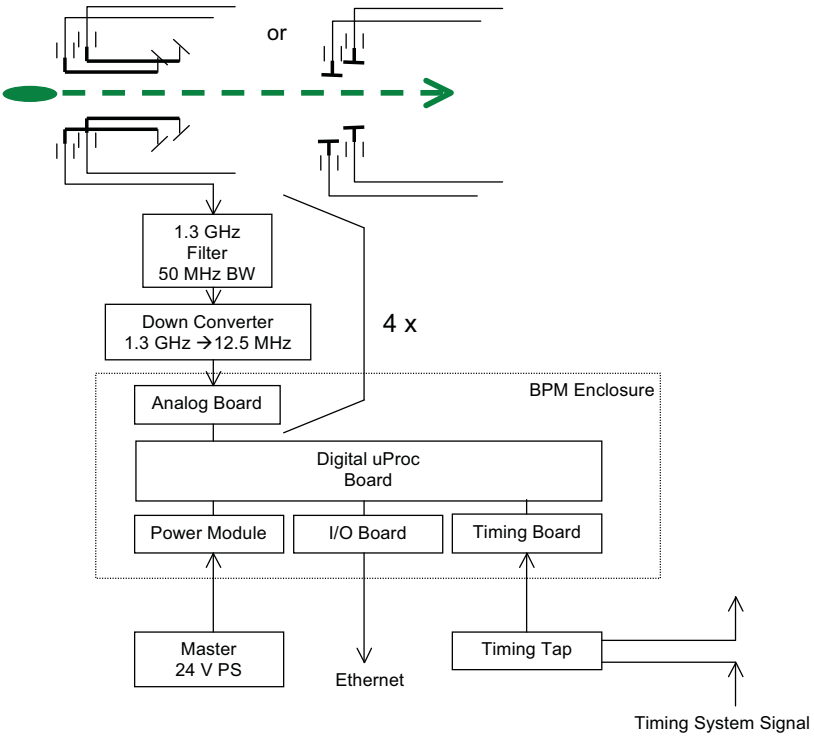

Figure 2.10.1: Block diagram of a beam position monitoring system.

at 50 MHz and an I/Q (amplitude and phase) measurement is performed. From the relative amplitudes of the 4 BPM signals the beam's position will be inferred.

The Digital Signal Processor (DSP) will provide average position results, timing error correction and other diagnostic information at various update rates ranging from 10 Hz to 10 kHz. The expectation is that the control system will be able to access this information at about a 10 Hz rate. As with the current CESR BPM system, the proposed BPM system will have the ability to acquire trajectory data triggered at 80 ns increments in a variety of timing patterns. The control of its timing system will be very flexible and will permit triggering of the trajectory data acquisitions locked to triggers of other instrumentation.

The position sensitivity for a stripline composed of four equally spaced strips around the circumference of a beam pipe of radius R is determined by the relative signals on each stripline. Using a beam displaced in the same plane as two diametrically oppositely spaced strips, the sensitivity can be estimated from the ratio of the difference voltage V_Δ and the sum voltage V_Σ from the strips to be proportional to the 'measured' x position,

$$x_\mathrm{m} = \frac{R}{2}\frac{V_\Delta}{V_\Sigma}\,.$$

The ratio of the difference over sum of 0.1 % would correspond to a 'measured' x position of 6.3 μm for the proposed stripline parameters for the ERL.

Table 2.10.1: Comparison of the expected resolution of stripline and button BPM detectors under various beam conditions. TN: thermal noise.

Operation Mode	Measurement Bandwidth	Stripline BPM Resolution (μm)	Button BPM Resolution (μm)
CW operation or	12.5 MHz	1.9	6.5
current ramp-up mode	10 kHz	0.17	0.58
1.3 GHz, 77 pC beam	10 Hz	0.005	0.018
	12.5 MHz (TN)	0.43	6.3
first turn trajectory mode,	240 Hz	17	160
240 Hz, 77 pC single bunch	240 Hz (TN)	11	160
first turn trajectory mode	12.5 MHz	2.7	25
240 Hz, 19 pC single bunch	10 kHz	0.23	2.2
	10 Hz	0.007	0.07
	12.5 MHz (TN)	1.7	25
first turn accelerator setup &			
low power energy recovery /	240 Hz	1.9	6.5
energy recovery accelerator setup	240 Hz (TN)	0.43	6.3
1.3 GHz, 77 pC, 240 Hz rep. rate,			
100 ns train duration			

Noise level and BPM resolution

The expected rms thermal noise voltage $V_{\rm n}$ is 3.2 mV for each of the BPM signals for the proposed stripline or button BPM system. After adding the two contributions in quadrature and including the fact that the automatic gain software will typically have the ADCs operating from 40-80 % of full scale, the noise level and resolution expected places a range for the position resolution of $1.4 - 2.5\,\mu$m for normal 1.3 GHz operation for the sampling of a single 12.5 MHz period. When averaging is employed, the average resolution will become $0.17\,\mu$m with a 10 kHz update rate or 5 nm with a 10 Hz update rate. Table 2.10.1 summarizes the expected resolution for the different modes of ERL operation.

System configuration for locations with two beams

In certain sections of the accelerator such as Linac A and B both the accelerating and decelerating beams will be present simultaneously. Measuring beam positions in these regions will raise some interesting challenges. The approach that has been adopted here uses the fact that the two beams will be equally spaced in time and thus produce a 2.6 GHz signal in addition to the normal 1.3 GHz signal. The relative amplitudes of these two frequency components are related to the charges in the accelerating and decelerating beams, q_A and q_D respectively, and the displacements of each beam, (Δx_A, Δy_A) and (Δx_D, Δy_D). The individual beam position information can then be extracted from the amplitudes and phases of the two frequency components.

2.10.3 Transverse beam stabilization

After accelerating the electron bunches to high energy, it is most important to deliver stable x-ray beams to the users. To avoid diluting the advantages of the low emittance beam, the position of the x-ray beam needs to be stable to better than 10 % of the x-ray beam size at the experiment, $\sigma_{\mathrm{x,x-ray}}$ and $\sigma_{\mathrm{y,x-ray}}$. The projection of the x-rays from the source point implies that the positional deviations (Δx, Δy) and angular deviations ($\Delta x'$, $\Delta y'$) of the electron beam's centroid at the source point must be held to 10 % of the standard deviations of its positional (σ_x, σ_y) and angular ($\sigma_{x'}$, $\sigma_{y'}$) distributions. If the electron beam has been stabilized against multi-pass beam breakup, then the next most serious effect will be centroid motion e.g. due to the variations from the laser driver, vibrations of the positions, or slow drifts in fields of accelerator elements and energy variations of the Linac RF accelerating fields. Feedback to precisely control the beam's trajectory through the ERL will be employed to counteract these deleterious effects.

To place a scale for the desired position stability, there are two cases to consider. The first is when the 77 pC bunches have a geometric emittance of 30 pm. In a region within the undulators where β_x and β_y are approximately 2.5 m, $\sigma_{x,y} = 8.4\,\mu$m and $\sigma_{x',y'} = 3.5\,\mu$rad, making the implied stability for $\Delta_{x,y} = 0.8\,\mu$m and for $\Delta_{x',y'} = 0.35\,\mu$rad. The second case is for the 19 pC high-coherence bunches, having the lower emittances of 8 pm. In the undulators with similar optics and beta functions, the beam sizes are $\sigma_{x,y} = 4.5\,\mu$m and $\sigma_{x',y'} = 1.8\,\mu$rad, and the stability requirements thus become $\Delta x, y = 0.4\,\mu$m, and $\Delta x', y' = 0.18\,\mu$rad. As an example if the beta-functions at the steering magnets were in a range from 5 m to 50 m, then the typical deflections to produce the minimum change just equal to $\Delta x, y = 0.4\,\mu$m and for $\Delta x', y' = 0.18\,\mu$rad would be in the range of $0.4\,\mu$rad to $4\,\mu$rad. With maximum steering strengths of ± 0.4 mrad for the ERL's corrector magnets, if these magnets are employed for feedback, they will need to be able to be set to less than $\pm 3 \times 10^{-4}$ of full scale.

Slow orbit feedback

The slow trajectory feedback is designed to correct the highest bandwidth position errors that are possible using the standard lower bandwidth steering correctors. If the slow position feedback system is configured using conventional laminated dipole magnets surrounding an aluminum beam pipe, the zero of the lead-lag compensation of the feedback loop should be set at the pole of the power supply and magnet transfer function, which should be at the eddy current frequency for the magnet laminations and is of the order of 60-100 Hz. This determines the frequency for the zero, leaving the next lowest pole at the beam pipe's eddy current roll-off frequency, which is 360 Hz for aluminum. This then becomes the unity gain frequency for the position feedback loop for a conventional single pole frequency roll-off, implying that the position feedback loop's bandwidth would be approximately 360 Hz.

If the source of the vibration's coupling to the beam occurs some distance away from particularly sensitive accelerator elements (e.g. the undulators) two or more position feedback clusters can be employed to suppress the motion of the beam due to the vibrations, and their effects would roughly multiply. Ultimately a detailed simulation study of slow trajectory will be undertaken to confirm this final feedback solution. In order to fully utilize the capability of the position feedback systems to stabilize the undulator beams, it will be necessary to have

steering power supplies with sufficient resolution (and this might require a second trim-steering winding and power supply for the correctors) and to have an accurate method of establishing the location of the BPMs relative to the x-ray experiment. The BPM locations may need to be determined either inertially or with a dynamical (e.g. laser-based) readout.

Lastly, there is one additional facet to the implementation of slow-position feedback for the ERL. It is likely that slow-trajectory feedback clusters will be enabled throughout the ERL in relatively few locations along the beamline because there may be no significant differential vibrational excitations of the beam and the feedback can, therefore, be disabled in that region. If this is the case, then the regions not enabled will still be susceptible to possible longer-term drifts in magnet fields, magnet supports, or stray fields. A solution to these long-term sources for trajectory drifts will be to have the control system execute a slow feedback loop (less than 1 Hz), which measures the beam's position throughout the entire trajectory, and make small changes to corrector magnets to restore the beam to a reference trajectory.

Fast orbit feedback

The preceding section described the slow-position feedback utilizing conventional steering magnets arranged in localized clusters with the BPMs from that region. As was shown above, this will give a slow feedback loop having an open loop gain with a single pole roll-off and a unity gain frequency of approximately 360 Hz. To anticipate the possibility of sources for beam motion at higher frequencies, wider bandwidth feedback is envisioned. Examples of possible higher frequency sources for beam motion are 1) oscillations in the Gun HV PS, 2) changes in beam loading of the RF accelerator cavities due to small photo-emission variations of the gun, caused by intensity variations of the laser, or 3) residual trajectory errors after the RF cavities' energy feedback loops have corrected phasing errors of the Linac's accelerating voltage.

The bandwidth of the general slow-trajectory feedback scheme proposed in the two preceding sections is limited by two separate effects: the eddy currents in the steering magnet's laminations and eddy currents in the vacuum chambers. Ferrite magnets acting on the beam through coated ceramic vacuum chambers or stripline kickers can overcome this. Installing a set of these deflection elements in both the horizontal and vertical planes along with BPMs in a similar clustered configuration as described for the slow trajectory feedback will allow a fast trajectory feedback loop with a bandwidth exceeding 100 kHz.

Control of beam position in the injector

The diagnostics in the injector will be comprised of devices that can be categorized into two classes: the diagnostics suitable for CW high average current beam and interceptive diagnostics usable with a low-power tune-up beam. The CW diagnostics will provide the necessary information on the beam centroids (two transverse positions, time of arrival and energy), bunch charge, and beam current, whereas the interceptive diagnostics will allow measurements of the second moments of the beam distributions as well as the phase space density maps of the pulsed beam containing the full bunch charge. Two additional types of devices will be used to monitor parameters of the full power beams. A THz spectrometer using the radiation from the dipole magnet in the merger will provide estimates of the longitudinal form-factor of the bunch and the flying wire will provide beam profile measurements under the

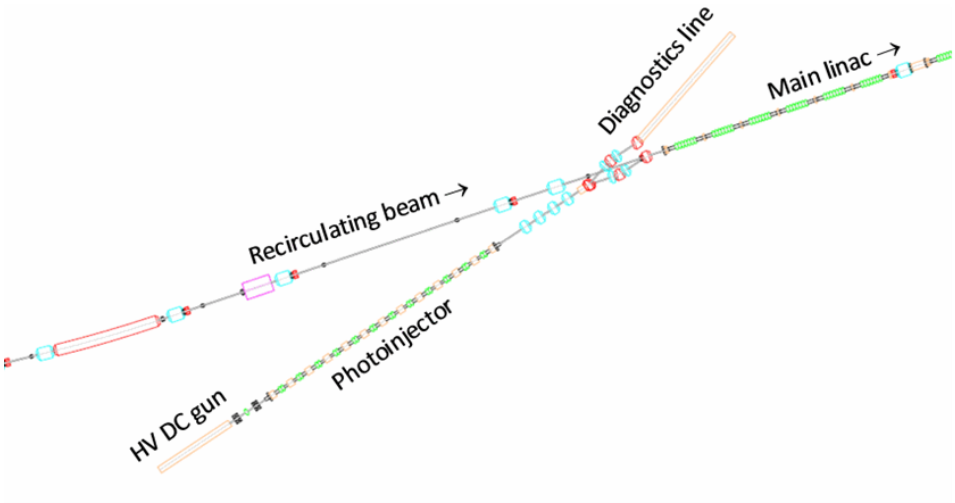

Figure 2.10.2: The location of the diagnostics beamline used for tune up of the injector at its full charge per bunch.

conditions of the full average current operation. The flying wire (20 micron diameter carbon filament moving transversely through the beam once with up to 20 m/s speed), although not non-interceptive in its nature, will minimally perturb the high-current beam and will be used occasionally during the machine setup stage at sufficiently high average current ($> 10\,\mathrm{mA}$).

Since the beam in the injector is space-charge dominated even at the design energy of about 15 MeV, it will be necessary to characterize the phase space prior to the injection into the main Linac. In the low-energy range of the injector, by far the most reliable method of assessing the transverse phase space density is through beam collimation by precision slits in order to convert the beamlet from space charge to emittance-dominated regime for subsequent probing to determine its intrinsic divergence. In order to characterize the beam under the conditions identical to those of the actual operation, a diagnostics line will be introduced symmetrically mirroring the main Linac arrangement (see Fig. 2.10.2). The first merger dipole can be used to switch the beam into the diagnostics line, which contains beam profile monitors, emittance measurement system, and longitudinal phase space characterization capability. These will all be suitable for full bunch charge characterization at a much reduced duty factor (the average beam current is less than 100 uA to limit the total beam power to about 1 kW).

2.10.4 Beam position and arrival time monitors

The primary diagnostics for monitoring the beam position and arrival time will be stripline BPMs, successfully deployed during Phase 1a photoinjector development stage. The photoinjector is equipped with 10 BPMs. The resolution of a 100 Hz data stream for beam position is on the order of a few microns for nominal bunch charge operation, which is more than adequate for photoinjector needs. Additionally, all BPMs report arrival time phases relative to the 1.3 GHz reference signal with a 0.1° accuracy under typical operation conditions. Beam orbit and phases will be compared to the online model, which will be incorporated into the

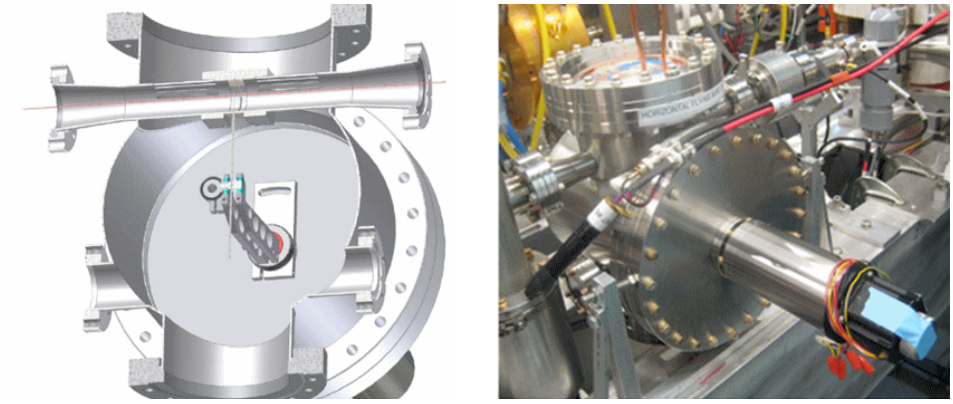

Figure 2.10.3: The cross-section of the flying wire profile monitor (left) and installation of the device in the Cornell ERL injector prototype (right).

control system.

2.10.5 Beam size

View screens with resolution of about 30 μm will be used to obtain the beam profile for the pulsed train tune up beam. Two different materials will be used to cover several orders of magnitude in beam current: BeO that is sensitive to sub-nano-Ampere average currents, and less sensitive CVD diamond screens that can take up to 1 μA of beam current. Each screen station will be equipped with both high- and low-sensitivity screens and interfaced to a 12-bit video camera serving the profile information to the control system. RF shielded assemblies will be employed throughout when the screens are retracted to minimize perturbations due to wakefields on the beam and heating effects.

Determining the transverse profile of the full average current beam is a challenging task. The MW level average power of the beam precludes interceptive techniques, while the low energy of the injector limits the usefulness of non-interceptive techniques analyzing the synchrotron radiation due to its rather long wavelength well outside the visible optical range. Possible approaches involve reduction of the 100 % duty factor beam with a very fast kicker into a dedicated diagnostics beamline equipped with a suite of interceptive diagnostics or the use of specialized diagnostics capable of withstanding the full MW power of the beam. A flying wire profile monitor (see Fig. 2.10.3) has been developed within the framework of the Phase 1a development work that allows the characterization of the full 100 mA average current beam. The system consists of a 20 μm carbon filament traversing the electron beam with a speed of up to 20 m/s. The filament causes scattering of a very small fraction of the electrons inside the bunch train with these electrons being lost on the beam pipe several meters downstream of the device and thus providing a signal proportional to the local density of the beam as intercepted by the filament. This diagnostics is intended for occasional use, primarily during the high average current beam setup. Further evaluation of this diagnostics approach is underway within the Phase 1b effort.

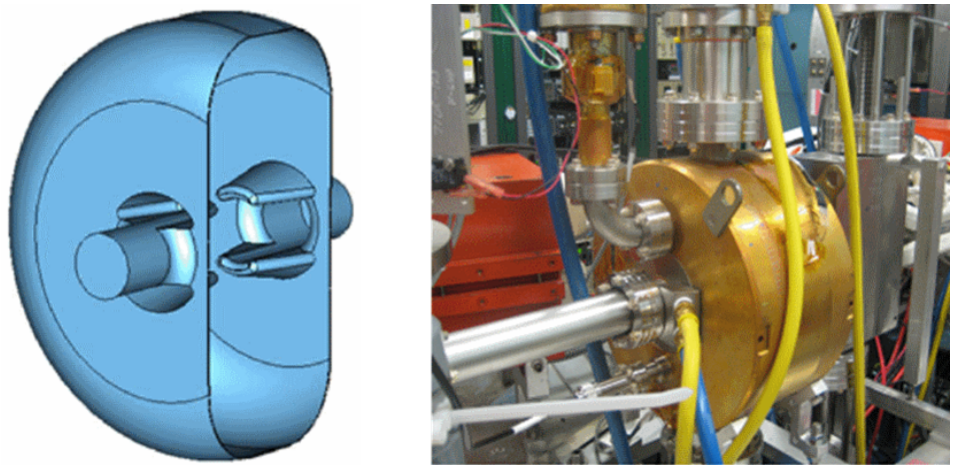

Figure 2.10.4: RF deflecting cavity used for temporal profile measurements in the injector. RF geometry (left) and installed device in the injector beamline (right).

Bunch length

A RF deflecting cavity (see Fig. 2.10.4) operating in $TM_{1,1,0}$-like mode at 1.3 GHz will be the primary diagnostics for the bunch length measurements [1]. The deflector is operated in pulsed mode consistent with the tune-up beam structure and low power requirement of the view screens downstream of the cavity used to register the streaked beam image. When not in use, the deflector will be detuned to avoid adverse effects on the beam. For better resolution, collimating slits can be used upstream of the cavity to increase the measurement resolution. Time resolution of about 100 fs has been demonstrated with the device in the Cornell ERL injector prototype. Additional collimation in the horizontal plane prior to the dipole magnets of the merger creating the dispersion allows direct mapping of the longitudinal phase space while simultaneously measuring the bunch length and the energy spread of transversely selected beam slice.

A THz spectrometer [2] picking up the radiation from the merger dipole will allow the characterization of the longitudinal profile form-factor for the full power beam in the bunch length region of interest (1-3 ps) . The spectrometer has been fully developed in the Phase 1a injector, and operational experience will be obtained within Phase 1b injector prototype operation.

Energy spread and fluctuations

Energy spread measurements will be carried out in the dispersive section of the merger. A beam dispersion of 0.3 m coupled with a collimated beam size of less than 100 μm (FWHM) will allow for a relative energy resolution of less than 10^{-3} for a given transverse slice as selected by the precision collimator. Likewise, energy fluctuations of less than 10^{-4} will be measurable with the BPMs located in the merger section.

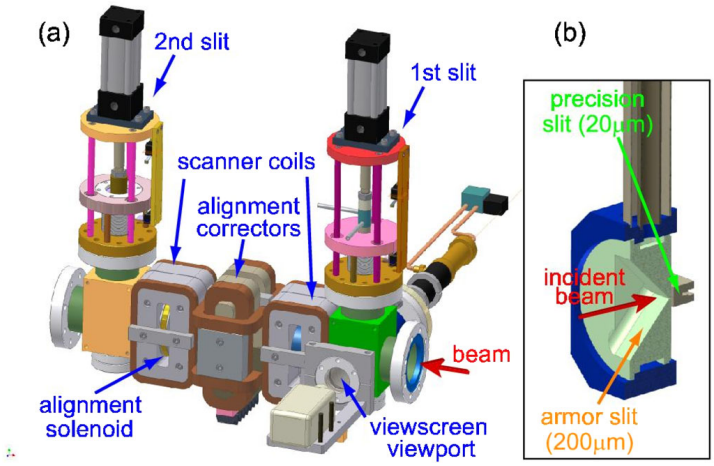

Figure 2.10.5: (a) Emittance measurement system as used downstream of the DC gun. The 15 MeV version of the device (not shown) is similar with the difference of a larger separation between the two slits (1.5 m). (b) details of one of the slits showing water cooled armor slit (80 μm opening for the 15 MeV version) protecting the precision slit.

Emittance

The emittance measurement system (see Fig. 2.10.5) will be comprised of precision slits (20 μm opening) and magnetic beam scanners. The signal is detected on a Faraday cup downstream of the second slit assembly. Avoiding mechanically moving parts will enable fast data acquisition at a several kHz rate, allowing detailed transverse phase space maps to be obtained in a matter of several seconds. A pair of the precision slits (both horizontal and vertical plane) will be located in the diagnostics beamline downstream of the merger, and the other set of retractable precision slits will be placed upstream of the deflecting cavity in the straight section following the injector cryomodule. Furthermore, each of the precision slits will be equipped with a special armor slit that dramatically reduces the beam power incident on the precision slit, thus, allowing the use of this diagnostics with about 1 kW of beam power or about 100 μA of average current. The resolution of the normalized emittance using this approach is better than 0.1 mm-mrad rms normalized [3].

Current measurement

A fast current measurement at a MHz rate is achieved using signals from a dedicated stripline BPM pickup. This fast signal will be used with the low-level RF control to compensate for the beam loading as well as with a dedicated feedback loop to stabilize the intensity of the laser. Slower precision measurements of the beam current will be accomplished using a DC current transformer having a noise level of a couple of μA over 1 s integration time.

Beam loss and halo measurement

A water-cooled movable copper edge will be used to determine the stray particle (halo) distribution both through detection of bremsstrahlung and direct current measurement from the isolated copper edge serving as a Faraday cup. A system to monitor beam scraping is planned that employes sensitive lock-in amplification capable of detecting nano-Ampere-level beam-current losses in the photoinjector. It will be similar to the one developed for the CEBAF accelerator [4].

Control of beam position for two beams in the ERL Linac

Having both an accelerated beam and a decelerated beam in the ERL Linacs will present special challenges for the beam position feedback. Since the steering corrector magnets planned for installation in the cryostat will be superconducting, it is not possible for these magnets to have sufficient bandwidth to develop trajectory feedback to stabilize ground vibrations, so this will require a different approach. The first step will be to measure the positions of each beam and then correct the trajectories of each beam separately by: 1) placing the trajectory of both beams on the axis of the Linac as nearly as possible, while accounting for the difference in energy of the beams; 2) putting more emphasis on the correction of the accelerated beam; and 3) adjusting the beams' incident trajectories before the merging of the two beams to reduce the differential orbit errors. One solution for the beam trajectory feedback in the Linacs will be to use fast and slow feedback clusters for each beam independently before their mergers upstream of both Linac-A and Linac-B and then to rely on slow orbit correction within the Linacs to reduce long-term trajectory drifts.

Control of beam parameters in undulators

The trajectory feedback cluster will in principle be capable of maintaining the beam's position and angle at both a source point within an undulator and at the end of the feedback cluster. Within the undulator regions of the accelerator, there are some outstanding design issues, which will need to be addressed. The first is that the spacing between adjacent undulators is relatively short; there is not a large phase advance and not many locations for BPMs or steering correctors. Between each undulator, it will be sufficient to utilize a pair of BPMs and a pair of horizontal and vertical steering correctors in a modified feedback configuration to stabilize any error induced upstream of the source point of the downstream undulator. However, it would be advisable for the redundancy of the position measurements to have at least three BPMs. Likewise, if the final optics design permitted a third horizontal and vertical corrector, spaced with a significant phase advance from the other two, these steerings could be viewed effectively as a backup set of correctors if one of the other two were to fail in service. In this proposed feedback implementation for the undulator regions, there will be one (or possibly two) position feedback clusters with the full set of BPMs and steerings upstream of the first of the south or north arc undulators. This feedback will stabilize the beam before it arrives at the first undulator. Between each of the next pairs of undulators, there will be the modified feedback configurations, which will be able to correct displacement and angle errors for each of the undulator source points.

The next question is: How will the beam stabilization be undertaken? One scheme is to separately stabilize the electron beam, using the ERL steering correctors, and the x-ray beam, using moveable gratings. However, if there is correlated motion remaining from the electron beam feedback, the x-ray beam feedback will need to correct this also. Another possibility is to take x-ray and electron beam position signals and connect them into a feedback matrix in the cluster feedback processor with appropriate weights and have them act on the electron beam's position to keep the x-ray beam on target. These two possibilities raise a significant concern in the ability to distinguish the core of the undulator beam from the much broader $1/\gamma$ fan of radiation. One approach would be to distinguish energy from power, perhaps by the use of a filter or by energy sensitive florescence that could be imaged with high resolution during the set-up procedures. Another possibility for the x-ray beamlines would be to establish either an inertial system as reference or perhaps a laser system as a reference for the BPMs. Determining which of these two viable solutions along with the appropriate instrumentation will be an important part of the final design optimization of the ERL.

2.10.6 Beam arrival time and experiment synchronization

Bunch arrival time measurements will be required at several locations within the accelerator in order to monitor and control the proper functioning of the energy recovery process as well as to provide a timing reference to the experimenters. The required resolution of these monitors depends strongly on the ERL operation mode. The design goal will be for a bunch arrival-time monitor resolution of about $1/10^{\text{th}}$ of the bunch duration, which corresponds to 200 fs (rms) for the 100 mA operation mode with its 2 ps (rms) long bunches, and 10 fs (rms) for the short bunch mode, which delivers bunches of less than 100 fs rms duration. This resolution should be achieved in a measurement bandwidth of at least 1 MHz so that these monitors can be utilized in fast control loops to stabilize the bunch arrival time. Ideally, the monitors will be capable of measuring the arrival times of single bunches, since this would allow for the study of high frequency noise contributions. This can be helpful to further improve the machine stability as well as to understand fast beam instabilities.

The resolution of the beam arrival-time measurement resolution will be degraded by two contributions: the distribution of the time-reference signal to the locations in the accelerator where the measurements take place; and the resolution limit of the beam arrival-time detection itself. The easiest approach for the arrival-time detection would be a scheme in which a beam-induced RF signal is mixed against a reference RF signal that will allow for resolutions of better than 50 fs. If very high frequencies are used for the phase detection process, even sub-10 fs resolution is feasible (see, e.g., [5]). The main difficulty with such a scheme is, however, the stable distribution of the reference RF signal within the accelerator. Even with very tight RF cable temperature control and with specially selected cable types with low thermal coefficients, the timing from the reference signals can easily drift by several picoseconds when cable lengths reach many hundred meters. As a result, an active way of measuring and controlling the travel times through the cables would be required.

An alternative approach of distributing the timing signals is to use the optical signal from a laser as a timing reference and to distribute this signal via optical fibers. The advantage of such a scheme is the fact that optical timing detectors allow for much better resolution than is achievable with RF technology. At the Sub-Picosecond Pulse Source (SPPS), the

timing reference of a laser was used to synchronize two color pump-probe experiments at an accelerator-driven light source for the first time. The electron bunch arrival time was measured with pulses from a Ti:Sapphire laser using electro-optical methods. The same laser was used as the pump source of the experiments. The time stamps derived from these arrival-time measurements reduced the arrival time jitter in the post-analysis to around 60 fs [6].

X-ray free-electron lasers that are capable of producing light pulses much shorter than 10 fs [7, 8] have initiated research on optical synchronization schemes that can deliver sub-10 fs precision. Two different approaches currently exist. In the first, the fiber length is stabilized based on an interferometric scheme that uses the narrowband optical frequency of a continuous-wave laser [9]. RF signals can be distributed over this stabilized link by RF modulation of the amplitude of the laser signal. At the end of the fiber link, the RF signal is extracted from the laser signal and can be used for synchronization purposes. In the second scheme, a mode-locked laser is used as a time reference and the optical fibers by which the signals are transmitted are stabilized based on optical cross-correlation between pulses from the laser and those reflected back at the end of the fiber link [10]. In this approach, the laser pulses from the fiber links can be utilized to drive an electro-optical detection scheme without the need for any additional intermediate systems, that might degrade the timing stability. This allows for measurements of the bunch arrival time with respect to the reference laser with a resolution of better than 10 fs [11]. This is currently the best reported resolution for an arrival-time measurement with respect to a remotely located time reference. The ERL design will use a similar scheme to provide an arrival-time resolution of 10 fs that will be required for the experimental program.

Optical timing reference and femtosecond stable distribution of reference signals

Passively mode-locked, femtosecond lasers capable of producing laser pulses trains with a timing jitter of only a few femtoseconds at frequencies above a few kHz (see, e.g., [12, 13]) exist and are now commercially available (see, e.g., [14]). Laser-timing changes occurring at lower frequencies can be corrected for with piezo-electric transducers used to lock the laser repetition frequency to a long-term stable, low-noise RF reference frequency. In order to simplify the dispersion compensation of optical fibers, a laser with an Erbium-doped gain medium is used.

For the ERL the laser pulse train will be transmitted via an optical fiber to the remote location in the accelerator. Figure 2.10.6 shows the schematic setup to stabilize the travel time of the optical pulses through the fiber. At the end of the fiber-link, part of the laser power will be reflected by a Faraday rotating mirror. In an optical cross-correlator, changes of the travel-time through the fiber will be determined by measuring the timing between the returning pulses and those directly from the laser. Variations of the travel-time will then be compensated for by a piezo-electric fiber stretcher in combination with a motorized optical delay-stage.

Femtosecond resolution bunch arrival-time monitors

Figure 2.10.7 below illustrates the principle of the electro-optical bunch arrival-time monitor (BAM). The beam will induce a fast transient signal in a broadband beam pick-up, which will

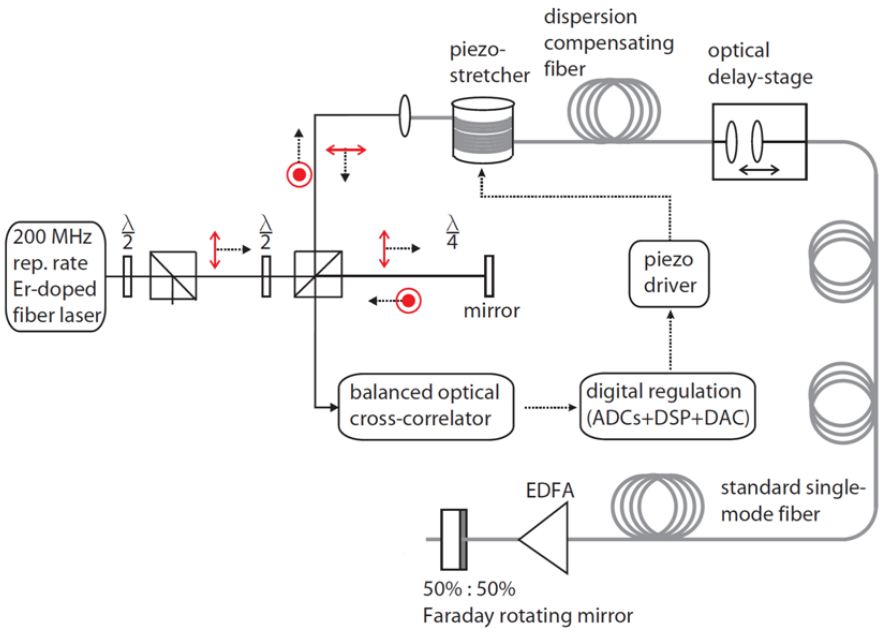

Figure 2.10.6: Schematic setup to stabilize the travel time of light pulses through an optical fiber with femtosecond precision (from [12]).

be used as the input of a Mach-Zehnder type electro-optical amplitude modulator (EOM). The timing of the reference laser will be adjusted in such a way that one pulse arrives at the time of the zero-crossing of the electrical signal when it passes the EOM. Electron bunch arrival time variations will shift the time of this zero-crossing and therefore lead to a different modulation voltage seen by the laser pulses and thus to varying laser-pulse energies after the EOM. By detecting the energy of individual laser pulses, the bunch arrival time can be deduced.

In order to reduce the dependence of the detection scheme on the electron bunch charge as well as to increase the dynamic range, a slow feedback loop with an optical delay line as an actuator will be used to keep the laser pulse near the zero-crossing of the transient signal even when the bunch arrival time changes. By this means, the dynamic range for slow beam arrival time changes will be limited only by the range of the delay line which can be many hundred picoseconds (around 360 ps in [12]). The dynamic range for fast timing changes will be limited to around 3 to 4 ps. This range can be extended by adding a second EOM that is driven by a strongly attenuated RF signal (see Fig. 2.10.8).

In the ERL, two new difficulties arise compared to the FLASH system [11, 12] that will require further research. The first one is the lower bunch charge of the ERL (77 pC or 25 pC), depending on the operation mode, which will be 10 to 30 times lower than in [11]. In order to maintain the same single bunch resolution, a modified beam pick-up will be required. If an arrival-time resolution of 10 fs is not required on a bunch-by-bunch basis but only in a bandwidth of 1 MHz, this will relax the required single bunch resolution by a factor of 36 since the results for many bunches can be averaged.

The second difficulty originates from the high repetition rate of the ERL. Ringing of the beam pick-up signal longer than the bunch spacing of 770 ps can degrade the measurement

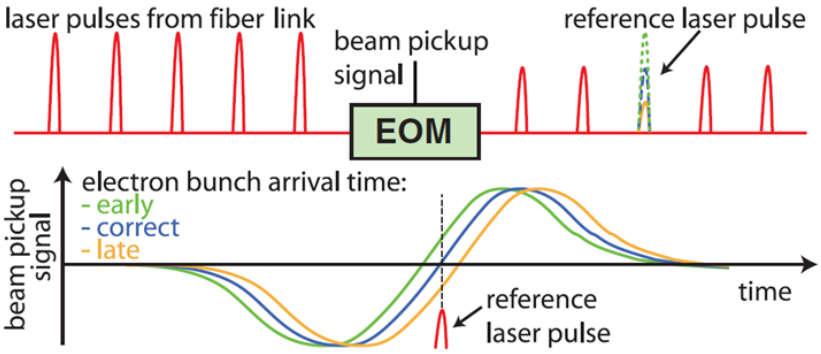

Figure 2.10.7: Principle of the electro-optical bunch arrival-time monitor (BAM). The amplitude of the reference lasers pulse train is modulated inside of an electro-optical modulator (EOM) driven by the signal of a fast beam pick-up. The electron bunch arrival time is then deduced from the laser amplitude (from [11]).

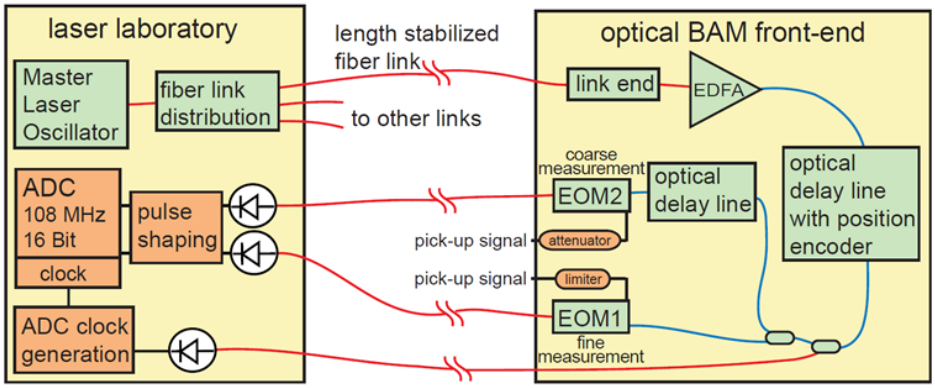

Figure 2.10.8: Schematic setup of the electro-optical detection scheme of the bunch arrival-time monitor (BAM) as it was used in first prototypes at FLASH (see [12]).

resolution. Even more important is the fact that due to the electron bunch rate, all laser pulses will be modulated in their pulse energies. This eliminates the possibility of normalizing the energy of a laser pulse modulated by the beam to that of a preceding, unmodulated pulse as used in [11, 12]. This normalization acts like a high pass filter and eliminates the influence of laser power variations as well as of ground currents in the beam pipe. A possible solution to account for laser amplitude variations would be to split the laser signal before it enters the EOMs and to measure the pulse energies of the unmodulated pulses separately. The influence of ground currents in the beam pipe can be reduced by high pass filtering the beam pick-up signal.

These issues will be resolved as part of the on-going ERL research and development program.

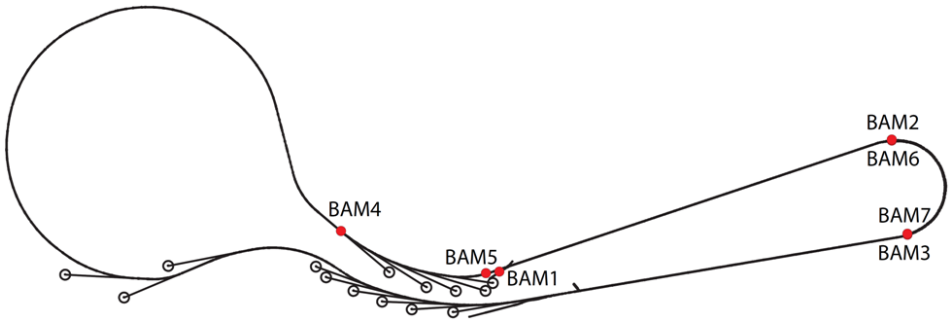

Figure 2.10.9: Important locations for the bunch arrival-time monitors (BAMs) along the ERL.

Placement of bunch arrival-time monitors and bunch arrival-time control

The most important locations at which bunch arrival-time monitors (BAMs) are required are illustrated in Fig. 2.10.9. The locations are chosen such that no arrival-time measurements take place at locations in which the accelerating and decelerating beam are superimposed.

BAM1 will measure the injection time into Linac A and BAM3 will measure the injection time into Linac B for the accelerating beam. BAM4 will be located close to the experimental beam lines in the north arc to provide the arrival-time of the compressed electron bunches to the experiments. BAM5 and BAM7 will measure the injection time for the decelerating beam into both Linacs.

The combination of two adjacent BAMs can be used for high resolution time-of-flight measurements for the accelerator section between both BAMs. By modulating the beam energy, also the R_{56} transport matrix element can be determined with high resolution using

$$R_{56} = \Delta t \cdot c \cdot \frac{E}{\Delta E} \,,$$

where c is the speed of light, E the beam energy, and ΔE the beam energy modulation.

BAM2 provides redundant information to BAM1 but it is placed after the injection merger so that the residual R_{56} element of the merger can be measured. BAM6 can isolate time-of-flight / R_{56} element changes in the turnaround.

Femtosecond stable synchronization of lasers for experiments

Experimental lasers (and also the injector laser) can be synchronized to the optical time reference laser by means of (two-color) optical cross-correlation. Potentially, such schemes will allow synchronizing both lasers to sub-fsec levels [15].

RF reference signals for cavity regulation

For ERL operating modes that do not longitudinally compress the electron bunches, the beam will be accelerated on the crest of the sinusoidal RF cavity field. This will result in a relaxed phase stability requirement for the cavity fields. For the case that the timing changes of all cavities are statistically independent, the beam energy spread will not be affected by RF phase

fluctuations. Systematic drifts of all RF cavity phases by ±0.5 deg will only lead to an increase in the beam energy spread of around 20 %.

The demands on the phase stability will be significantly increased for the cases in which the electron bunches are longitudinally compressed. One of the most sensitive parameters affected by the variation of the cavity RF phases is the bunch arrival time. A phase variation of the combined field of all cavities by 0.005 deg will lead to an arrival-time shift of 10 fs, which is the required arrival-time stability in the bunch compression modes. In the case of statistically independent phase fluctuations of all 384 cavities, this leads to a phase stability requirement of around 0.1 deg (or a corresponding RF timing variation of $\sim 200\,\mathrm{fs}$) for each cavity. Over longer time periods, this stability requirement reaches the limit of what has been achieved with conventional RF based timing systems. With optical timing systems, significantly better stability has been achieved [9, 16]; however, these systems have a limited number of end points and the performance may degrade with the number of end points needed for the ERL. The total cost for such a large optical synchronization system may also be high. Further research and development will provide the needed information for the decision as to the optimal path for providing the needed cavity regulation.

Beam arrival time and bunch compression stabilization

It may be possible to significantly reduce the requirements on the RF reference signal stability by using beam-based methods to measure the bunch compression as well as the bunch arrival-time. This information could then be used to perform correction of the phases and field amplitudes of several adjacent cavities [11]. Possible monitors that could be used in such a longitudinal feedback system would be BAMs or BPMs in a dispersive section for beam energy measurements and bunch compression monitors (BCM). These would provide measurements of the beam phase.

The feedback can then either act only on the superconducting cavities in the main Linacs, or could also act in addition on dedicated normal-conducting feedback cavities. The second approach provides the possibility of operating at a much larger feedback bandwidth compared to the superconducting cavities because of their much shorter filling time. Estimates of the required power and accelerating gradient for these normal conducting cavities are underway.

2.10.7 Longitudinal beam profile measurement

Electro-optical systems, transverse deflecting cavities, and the measurement of beam-induced diffraction radiation will be used to measure the longitudinal beam profile in the ERL.

Electro-optical schemes

Various electro-optical schemes have been developed for measurements of the longitudinal bunch profile [6, 17–19]. Because of the reduced complexity of the methods described in [17] and [19], one of these two schemes will be used in the ERL.

Figure 2.10.10 shows the operation of the 'spectral decoding' scheme [17]. A broadband laser pulse is linearly chirped and sent through an electro-optically active crystal in the beam pipe, where it co-propagates with an electron bunch. The coulomb field of the electron beam leads to a polarization rotation of the laser pulse inside of the electro-optical crystal. After

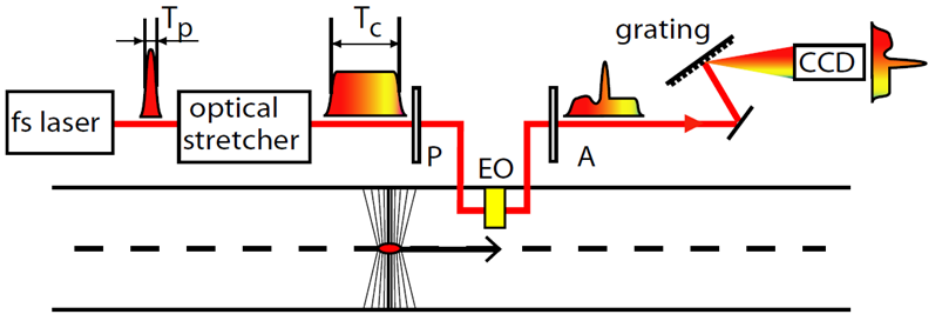

Figure 2.10.10: A typical layout for an electro-optical system for measuring the longitudinal beam profile [20]

a polarizer, these polarization changes are converted into an intensity modulation, which is measured with a spectrometer. By this, the longitudinal shape of the coulomb field can be determined and thus the longitudinal bunch shape. The resolution of this method is limited to around 100 fs, mainly due to phonon resonances inside of the electro-optical crystals as well as due to the generation of intensity sidebands after the final polarizer.

A second scheme [19] uses a similar setup, but in contrast to the first scheme, a very narrowband laser pulse (or even a CW laser) is used. The polarization rotation induced by the electron bunch inside of the electro-optical crystal leads to spectral sidebands, which again are measured with a spectrometer. While the first method measures the temporal beam profile, this method determined the frequency spectrum of the electron bunch and potentially, much shorter structures than 100 fs can be measured.

Both schemes have the advantage that they are non-destructive and that they would work at full beam current in the ERL. The effect of a high-current beam on the properties of the crystal might be a potential problem. This will be studied as part of the ongoing ERL research and development program.

Transverse deflecting structures

Transverse deflecting structures (TDS) currently provide the best longitudinal bunch shape resolution. The typical setup is shown in Fig. 2.10.11. Inside of the structure, the electron beam receives a time-dependent kick, which is measured with a beam profile monitor. The time resolution can be better than 20 fs [21, 22] and in combination with a dispersive section the longitudinal phase space distribution can also be determined from the temporal beam profile. By combining this with quadrupole scan techniques, the slice emittance along the beam bunch can also be measured.

The pulsed deflecting RF field in the TDS would require pulsed operation of the ERL and will be used mainly as an instrument for tuning and understanding the beam transfer through the accelerator. In combination with a very fast kicker and a septum magnet, an online measurement of the longitudinal phase space might be feasible in special cases.

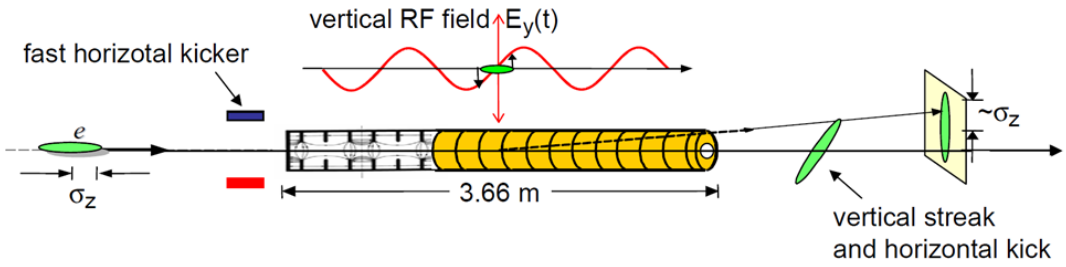

Figure 2.10.11: Typical transverse deflecting structure system for measuring the longitudinal bunch shape.

Diffraction radiation based monitors

Diffraction radiation, which is emitted when the electron bunches traverse a metallic slit or pin-hole, can also provide a tool for monitoring changes in the longitudinal bunch profile. In the simplest case, the integrated intensity of the emitted THz radiation is measured. Bunch length variations change the longitudinal form factor and thus the radiation intensity. The simplicity of this scheme make this bunch compression monitor ideally suited for a beam-based feedback system [11].

Even more information about the bunch shape can be determined by analyzing the THz radiation with a spectrometer [23].

This approach could provide a cost-effective method for providing continuous measurements for a beam-based feedback system. The concern is the possible effect on the beam emittance due to possible HOM generation by the structure. Simulations will be carried out to understand the importance of this possible effect.

2.10.8 Diagnostics in the main Linac

Multiple monitor emittance diagnostics

A multiple monitor emittance measurement system will be installed after the main Linac and before the beam enters the undulator sections. The system will verify the emittance minimization scheme used in the injector. It is important to do the measurements at this location since the emittance measurements after the injection merger take place at an energy of 15 MeV and space-charge effects within the first acceleration module of the main Linac can cause the beam emittance to change.

The system will also be used to study the potential beam emittance degradation due to beam transport through the two main Linacs and the first turn-around loop. Possible sources for emittance degradation are incoherent and coherent synchrotron radiation as well as ion accumulation effects. Simulations predict that all of these effects have limited impact on the beam emittance; however, ions trapped within the beam pipe can defocus the beam and therefore modify the Twiss parameters compared to the design parameters. This would lead to a beta-beat within the undulator sections and thus to increased x-ray beam sizes at the experimental stations.

A multi monitor emittance measurement system equipped with viewscreens as well as with

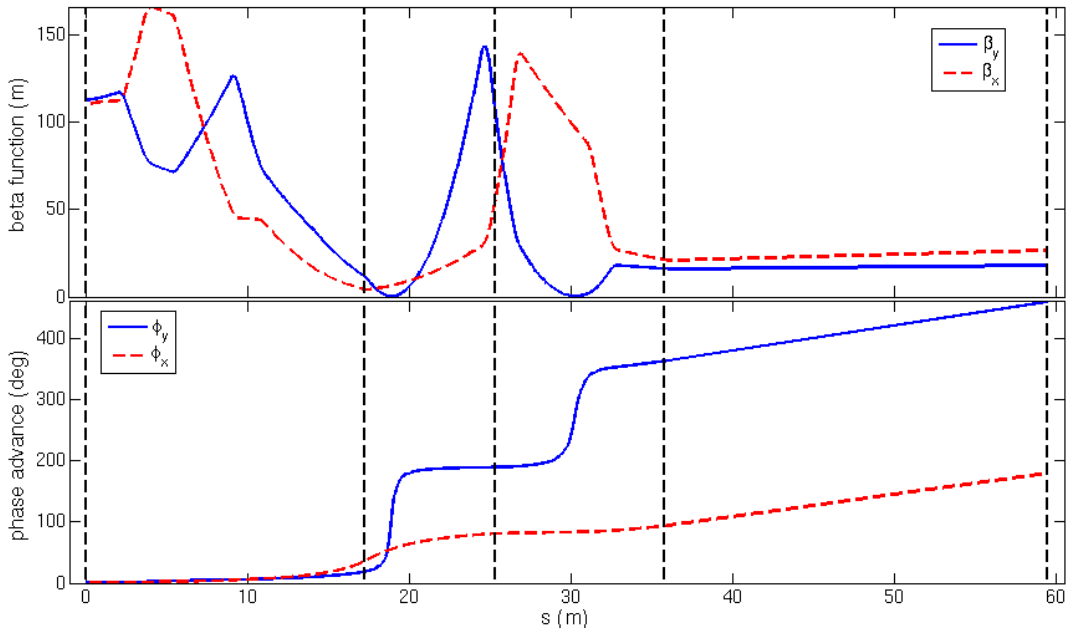

Figure 2.10.12: Beta functions and phase advance in the south-arc section of the ERL. The dashed lines indicate the locations at which beam profile monitors should be located for measurements of the beam emittance and Twiss parameters.

high-speed wire scanners will provide beam size measurements for low- as well as for high-beam currents. By optimizing the monitor placement as well as the beam optics, the beam phase space ellipses can be determined from the measured beam sizes, giving the transverse beam emittances as well as the Twiss parameters.

Due to the ultra-low beam emittance and the resulting small spot sizes, beam size measurements at full beam energy are challenging. To achieve reasonable beam size measurements with the limited resolution provided by state-of-the-art Optical Transition Radiation (OTR) viewscreens and wire scanners, large beta functions at the locations of the monitors are preferable. The calculations to determine the beam emittance as well as the beam Twiss parameters, however, also require a more or less homogeneous coverage of a 180 degree phase advance in both transverse planes. Elsewhere, this can be performed by appropriately positioning three screens in a drift space in which the beta-functions have a waist [24] or by using four beam size monitors within a FODO lattice [25].

In order to save space and still allow for accurate measurements, an optimized configuration that uses five monitors distributed within the south-arc section right after the main Linac has been studied. Figure 2.10.12 shows the placement of the monitors and the corresponding design lattice functions. The fifth monitor is located after the first undulator in order to provide higher resolution in the horizontal plane without modifying the existing beam optics.

The resolution for the beam emittance measurement as well as for the Twiss parameters was analyzed using methods described in [26]. A beam size resolution given by the rms of a 5 μm rms monitor resolution and 10 % of the beam size at the monitor location was assumed. For the layout shown in Fig. 2.10.12 this resulted in an emittance uncertainty of around 20 %

in the vertical plane and 25 % in the horizontal plane assuming a normalized beam emittance of 0.3 mm-mrad in both planes.

X-ray based online beam size monitoring

X-ray based beam size monitors will be used to observe emittance or beam optics variations during operation. A variety of high resolution methods exist (see, e.g., [27–30]), which have been extensively studied at third-generation light sources. Amongst those methods are pin-hole and pin-hole array x-ray monitors, as well as observation of the vertically polarized optical synchroton radiation at PSI in Switzerland. Beam size resolutions of better than 2 μm have be achieved.

When the beam Twiss parameters are known, a single beam size measurement in a section with no dispersion is sufficient to measure the beam emittance. In the presence of horizontal dispersion, two measurements are required. These systems will be installed in both turnaround arcs, as well as in the CESR ring. The required beam Twiss parameters will be provided by initial measurements with the emittance measurement systems in the injector as well as in the south arc.

Beam current measurements

The beam current signal along the accelerator will be provided by the BPM system. At several locations, a high dynamic-range bunch-charge monitor, based on the signal of a stripline pick-up and a logarithmic power detection will be used. A DC transformer will be used for the absolute beam current measurement.

Energy spread measurements

Wire scanners and screens in the dispersive section in the two turnarounds, as well as inside CESR, will be used for the energy spread measurements. In a section with a horizontal dispersion of 0.5 m, which can be generated at several locations, beam size monitors with a 5 μm resolution will provide an energy resolution of $\delta E/E = 10^{-5}$ for a sufficiently small horizontal beta function. This is more than sufficient to measure and verify the design energy spread of 2×10^{-4} for the entire beam and will also - albeit limited in resolution - allow for measurements of the slice energy spread. By having both wire scanners and screens, the energy spread will be studied at low- as well as at high-beam currents.

Beam loss measurements

The requirements for the beam loss monitoring systems for the ERL are challenging. The conventional technique of simply measuring the beam current at two different locations in the machine and taking the difference of the two measurements to find the loss is not possible with current technology. In the insertion device region, the losses have to be limited to 1 pA out of 100 mA and 1 nA for the rest of the machine and would require a part in 10^{11} and 10^{8} sensitivity respectively. To achieve the needed sensitivity, the radiation from the lost beam particles must be measured locally.

Ionization chambers are the most robust devices to measure radiation loss but have limited sensitivity [31]. PIN diodes provide more sensitivity but may be prone to radiation damage in the higher radiation areas [32]. Cherenkov counters consisting of a radiator viewed by a photomultiplier [33] can be fairly robust in terms of radiation damage and have better sensitivity than PIN diodes. The most sensitive detectors are bulk sciintillators [34] viewed by photomultipliers but the bulk scintillators are subject to radiation damage in varying degrees depending on the scintillating material.

The final design for the ERL beam loss monitoring system will be a combination of all of these techniques tailored to the requirements for each of the regions of the machine.

2.10.9 Seismic Environment

Data on the motion of the quadrupoles in CESR have been obtained under a variety of conditions. A geotechnical consultant, Terrascience Systems, Ltd., has taken extensive measurements in and around two test borings near the turn-around ends of the main Linacs. Data from the LIGO site at Hanford Washington have also been analyzed especially with respect to vehicle traffic on a nearby highway.

The conclusions from the LIGO studies [35] are that:

1. The largest semi-continuous off-site seismic signal in the 1 to 50 Hz band is produced by traffic on the surrounding roads.

2. Seismic motion from trucks can be greater than 10 nm at the nearest stations. Motions from cars are usually less than 1 nm.

3. Experiments with site vehicles suggest that the seismic frequency is given by the velocity and axle-spacing of the vehicle (see Fig. 2.10.13).

4. Signal propagation velocities are in the range of $450 \pm 25\,\mathrm{m/s}$.

5. Tamper signals travel at about $300\,\mathrm{m/s}$ at 10 Hz and about 75 m/s at 50 Hz.

6. Q of the vibration produced by several trucks in the 4.4 to 6 Hz range was ~ 70.

7. Typical amplification by the building structure is a factor of 2 to 3.

The results from the Terrasciences Systems tests [36] indicate that the geotechnical conditions at the ERL site have eigen-frequency peak responses in the 4 to 6 Hz region. This is in the middle of the spectrum generated by typical truck traffic. Their measurements for one-hour periods during the tests are given in Fig. 2.10.14.

To convert these velocity spectra to amplitude spectra in order to compare with the LIGO results requires multiplying by $1/f^2$. The distance to Route 366 from the test site is about 100 m and it is about 20 m from Judd Falls Road.

Vibration amplitude measurements using a sensitive accelerometer (Wilcoxon Model No. 731A/P31 with a bandwidth of 0.1 to 450 Hz) of the CESR tunnel floor and of a typical quadrupole magnet frame in the CESR ring are given in Fig. 2.10.15. The cross-tunnel trace is the quietest place in CESR in terms of seismic noise.

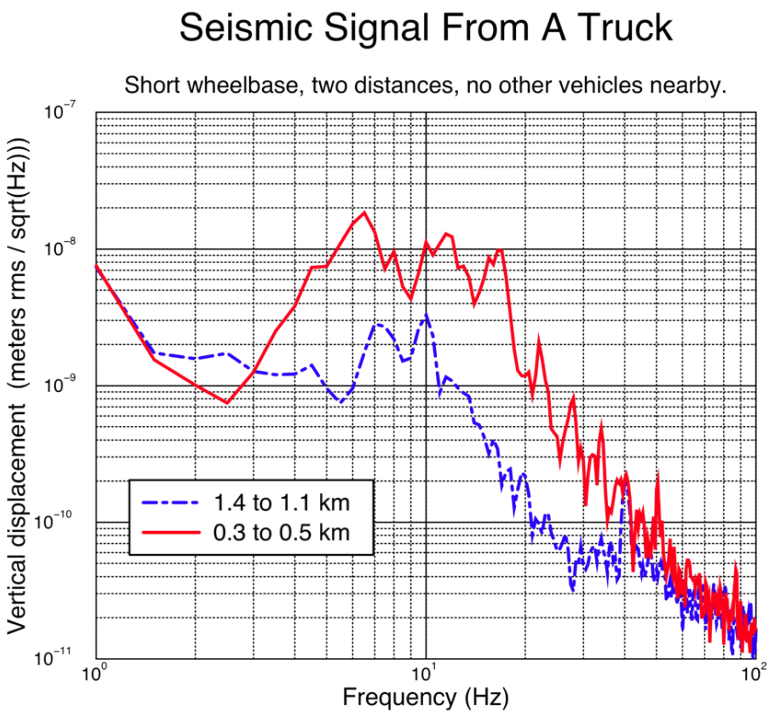

Figure 2.10.13: Seismic signal from a truck on the highway near LIGO site at Hanford Washington. Signal measured in test pits near the LIGO interferometer.

These vibration spectra can form the basis for determining the necessary isolation of sensitive machine components to meet the stringent ERL beam stability requirements. In most cases only modest improvement will be needed. For the undulator region, beam based-feedback can be used to provide the needed stability of the x-ray beams. The engineering requirements for this feedback are easily met with current technology.

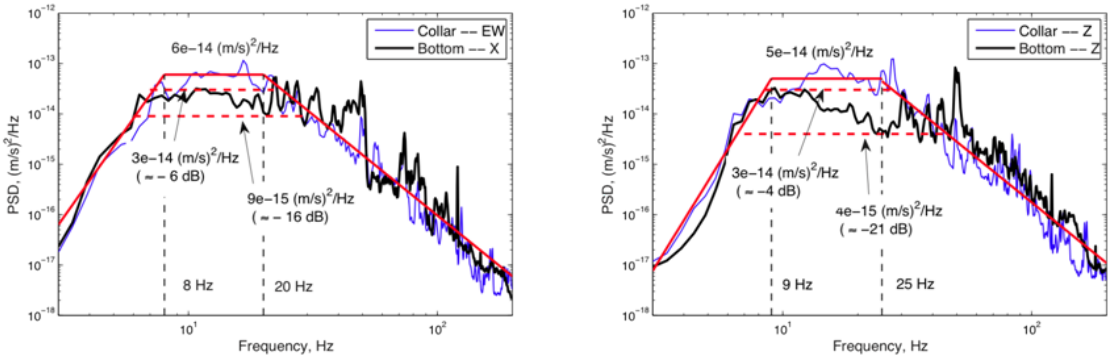

Figure 2.10.14: Velocity spectra measured by Terrasciences Systems near the proposed ERL site.

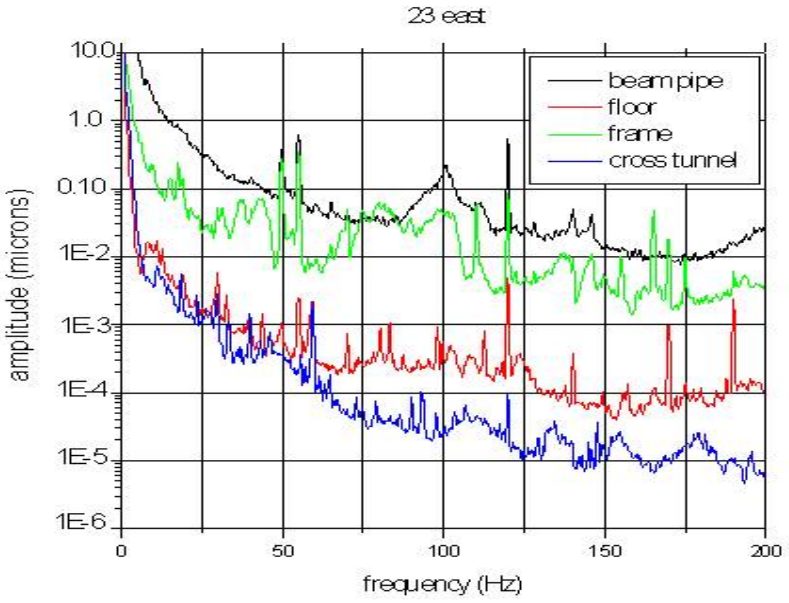

Figure 2.10.15: Results from vibration amplitude measurements in various locations in the CESR storage ring. The trace labeled frame is the frame that holds the quadrupole at this location. Cross tunnel is the floor of the diametric tunnel.

References

[1] Belomestnykh, S. *et al. Deflecting cavity for beam diagnostics at Cornell ERL injector.* Nucl. Instr. and Meth. A, **614**, pages 179–183 (2010).

[2] Schneider, G., *et al. Comparison of electron bunch asymmetry as measured by energy analysis and coherent transition radiation.* Phys. Rev. E, **56** (4), pages R3780–R3783 (Oct 1997). doi:10.1103/PhysRevE.56.R3780.

[3] Bazarov, I. V., *et al. Benchmarking of 3D space charge codes using direct phase space measurements from photoemission high voltage dc gun.* Phys. Rev. ST AB, **11** (100703) (2008).

[4] Allison, T., *et al. The CEBAF Beam Scraping Monitor.* In *Proceedings of the PAC 2001 Conference, Chicago, USA*, page 2389 (2001).

[5] Andersson, A. and J. P. H. Sladen. *First Tests of a Precision Beam Phase Measurement System in CTF3.* In *Proceedings of the PAC 2007 Conference, Albuquerque, USA* (2007).

[6] Cavalieri, A. L., *et al. Clocking Femtosecond X Rays.* Phys. Rev. Lett., **94** (11), page 114801 (Mar 2005). doi:10.1103/PhysRevLett.94.114801.

[7] *Operation of a free-electron laser from the extreme ultraviolet to the water window.* Nature Photonics, **1**, pages 336 – 342 (June 2007).

[8] Ding, Y. *et al. Measurements and Simulations of Ultra-Low Emittance and Ultra-Short Electron Beams in the Linac Coherent Light Source.* Technical Report SLAC-PUB-13525, SLAC (2009).

[9] Wilcox, R., *et al. Stable transmission of radio frequency signals on fiber links using interferometric delay sensing.* Opt. Lett., **34**, pages 3050–3052 (2009).

[10] Kim, J., *et al. Long-term femtosecond timing link stabilization using a single-crystal balanced cross correlator.* Opt. Lett., **32**, pages 1044–1046 (2007).

[11] Löhl, F., *et al. Electron Bunch Timing with Femtosecond Precision in a Superconducting Free-Electron Laser.* Phys. Rev. Lett., **104** (14), page 144801 (Apr 2010). doi:10.1103/PhysRevLett.104.144801.

[12] Löhl, F. *Optical Synchronization of a Free-Electron Laser with Femtosecond Precision.* Ph.D. thesis, University of Hamburg (2009).

[13] *Attosecond-resolution timing jitter characterization of free-running mode-locked lasers.* Opt. Lett., **32**, pages 3519–3521 (2007).

[14] Onefive GmbH. *Ultra low timing jitter performance & characterization of Origami femtosecond laser series.* White Paper P/N 09-001, Onefive GmbH (2009).

[15] *Attosecond active synchronization of passively mode-locked lasers using balanced cross-correlation.* Opt. Lett., **28**, pages 947–949 (2003).

[16] *Drift-free femtosecond timing synchronization of remote optical and microwave sources.* Nat. Photon, **2**, pages 733–736 (2008).

[17] Wilke, I., *et al. Single-Shot Electron-Beam Bunch Length Measurements.* Phys. Rev. Lett., **88** (12), page 124801 (Mar 2002). doi:10.1103/PhysRevLett.88.124801.

[18] Berden, G., *et al. Electro-Optic Technique with Improved Time Resolution for Real-Time, Nondestructive, Single-Shot Measurements of Femtosecond Electron Bunch Profiles.* Phys. Rev. Lett., **93** (11), page 114802 (Sep 2004). doi:10.1103/PhysRevLett.93.114802.

[19] Jamison, S. P., *et al. Upconversion of a relativistic Coulomb field terahertz pulse to the near infrared.* Appl. Phys. Lett., **96**, page 231114 (2010).

[20] Steffen, B. *Electro-optic methods for longitudinal bunch diagnostics at FLASH.* Ph.D. thesis, University of Hamburg (2007).

[21] Brachmann, A. *et al. Femtosecond Operation of the LCLS for user experiments.* In *Proceedings of the IPAC10 Conference, Kyoto, Japan* (2010).

[22] Röhrs, M., *et al. Time-resolved electron beam phase space tomography at a soft x-ray free-electron laser.* Phys. Rev. ST Accel. Beams, **12** (5), page 050704 (May 2009). doi: 10.1103/PhysRevSTAB.12.050704.

[23] Delsim-Hashemi, H. *Infrared single shot diagnostics for the longitudinal profile of the electron bunches at FLASH.* Ph.D. thesis, University of Hamburg (2008).

[24] Akre, R., *et al. Commissioning the Linac Coherent Light Source injector.* Phys. Rev. ST Accel. Beams, **11** (3), page 030703 (Mar 2008). doi:10.1103/PhysRevSTAB.11.030703.

[25] Löhl, F., *et al. Measurements of the transverse emittance at the FLASH injector at DESY.* Phys. Rev. ST Accel. Beams, **9** (9), page 092802 (Sep 2006). doi:10.1103/PhysRevSTAB. 9.092802.

[26] Löhl, F. *Measurements of the transverse emittance at the VUV-FEL.* Master's thesis, University of Hamburg (2005).

[27] Hofmann, A. *Electron and proton beam diagnostics with synchrotron radiation.* IEEE Transaction on Nuclear Science, **NS-28** (1981).

[28] Hofmann, A. and F. Meot. *Optical Resolution of Beam Cross-Section Measurements by means of Synchrotron Radiation.* Nucl. Inst. Meth., **203**, pages 483–493 (1982).

[29] *The geometry and optics of synchrotron radiation.* Particle Accelerators, **5**, page 199 (1973).

[30] Peatman, W. B. and K. Holldack. *Diagnostic front end for BESSY II.* J. Synchrotron Rad., **5**, page 639 (1998).

[31] Stockner, M. *et al. Classification of the LHC BLM Ionization Chamber.* In *Proceedings of DIPAC 2007 Conference, Venice, Italy* (2007).

[32] Juexina, L. *et al. Design of the Beam Loss Monitoring System in Strong Prompt Radiation Field.* Nucl. Instr. And Meth. A, **579**, pages 465–467 (2007).

[33] Gorodetzky, P. *et al. Quartz Fiber Calorimetry.* Nucl. Instr. And Meth. A, **361**, pages 161–179 (1995).

[34] Zorn, C. *A Pedestrian's Guide to Radiation Damage in Plastic Scintillators.* **32**, pages 377–383 (1993).

[35] Schofield, R. *Talk to LIGO Collaboration.*

[36] Zaicenco, A. Technical report, Terrascience Systems Ltd. (2010).